THE JOURNAL OF PHYSICAL CHEMISTRY Letters

LETTER

pubs.acs.org/JPCL

High Open Circuit Voltage Quantum Dot Sensitized Solar Cells Manufactured with ZnO Nanowire Arrays and Si/ZnO Branched Hierarchical Structures

P. Sudhagar,[†,⊥] Taeseup Song,[‡,⊥] Dong Hyun Lee,[‡] Iván Mora-Seró,[*,§] Juan Bisquert,[§] Michael Laudenslager,[∥] Wolfgang M. Sigmund,[†,∥] Won Il Park,[‡] Ungyu Paik,[*,†] and Yong Soo Kang[*,†]

[†]World Class University Program Department of Energy Engineering and Center for Next Generation Dye-Sensitized Solar Cells and [‡]Division of Materials Science Engineering, Hanyang University, Seoul 133-791, South Korea

[§]Photovoltaic and Optoelectronic Devices Group, Departament de Física, Universitat Jaume I, 12071 Castelló, Spain

[∥]Department of Materials Science and Engineering, University of Florida, Gainesville, Florida 32611−6400, United States

Supporting Information

ABSTRACT: Quantum dot sensitized solar cells (QDSCs) are currently receiving increasing attention as an alternative to conventional dyes. The efficiencies of QDSCs have experienced a fast growth in the last years, mainly due to an increase in the reported photocurrents and fill factors. Despite this increase, further enhancement of QDSCs needs an improvement of the obtained photovoltage, V_{oc}, being the current main challenge in these devices. Here we show that an appropriated nanostructure of wide band gap semiconductor electrode allows us to reduce the recombination process, with a significant enhancement of V_{oc}. V_{oc} as high as 0.77 V has been demonstrated for ZnO nanowires array electrodes. The performance of the cell can be even increased to a promising 3%, using a novel photoanode architecture of "pine tree" ZnO nanorods (NRs) on Si NWs hierarchical branched structure. Most importantly, we show the necessity of exploring new electrode architectures to improve the current efficiencies of QDSCs.

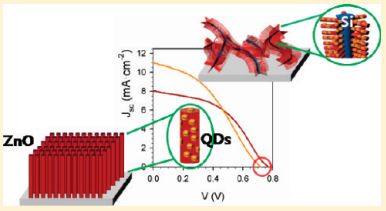

SECTION: Energy Conversion and Storage

Inorganic semiconductors are currently receiving increasing interest as light sensitizers for low-cost photovoltaic devices.[1−4] In the standard sensitized solar cell configuration,[5] a dye monolayer is used as a light-harvesting material from which electrons are injected into a nanostructured wide bang gap semiconductor (i.e., TiO_2, ZnO, SnO_2). The oxidized dye is regenerated by the donor species of a redox couple solved in an electrolyte, allowing an excellent wetting of the whole effective area of the nanostructured electrode. Finally, the electrolyte is regenerated in turn at the counter electrode by the complementary redox reaction. In this configuration, the nanostructured nature of the active electrode plays a key role in obtaining high efficiency devices because the increase in the effective surface allows higher dye loading amount and consequently an increase in the light harvesting. Efficiencies >11% have been obtained for dye-sensitized solar cells (DSCs).[6,7] Semiconductor quantum dots (QDs) as a light absorbing material in QD-sensitized solar cells (QDSCs) also awake great interest by their fascinating features. The QD band gap can be tuned, enabling us to tailor light absorption; they have a higher extinction coefficient than the conventional dyes,[8] large intrinsic dipole moment favoring charge separation,[9] and finally the multiple exciton generation process to increase the efficiency of QDSCs.[10]

Despite these potentials, the efficiency of QDSCs is significantly lower than DSCs,[11] being currently around 4 to 5% for liquid devices[12,13] and ∼5% for solid devices.[14] These efficiencies have been obtained after a fast growth of the efficiencies of QDSCs in the past few years mainly due to an increase in photocurrents, J_{sc}, and fill factors, *FF*. Photocurrent, using SnO_2 nanostructured electrodes and polysulfide electrolyte, as high as 17.4 mA/cm^2, has been reported for QDSCs.[15] *FF* of QDSCs is highly dependent on the electrolyte and counter electrode used. Values around 0.55 to 0.65 have been obtained with an electrolyte containing Co redox couples and the standard platinized counter electrode[16,17] and also with polysulfide redox couples using different counter electrodes.[12,13,18] Despite the increase obtained for J_{sc} and *FF* in QDSCs, the open circuit voltage, V_{oc}, the third determinant factor in solar cell efficiency, has not experienced an analogous enhancement, and it is the main current challenge for the optimization of QDSCs. V_{oc} is limited to values around 0.55 V or even lower, in most of the cases, when polysulfide electrolyte is used. Therefore the increase in V_{oc} is the main current challenge to increase the efficiency of QDSCs. There are very few examples of higher V_{oc} using polysulfide. V_{oc} of 0.69 and 0.64 V using CdS and CdS/CdSe QDSCs, respectively, were obtained with TiO_2 nanofibrous electrodes,[19] and V_{oc} = 0.71 V using CdSe as sensitizer and TiO_2 inverse opal as

Received: June 23, 2011
Accepted: July 20, 2011
Published: July 20, 2011

electrodes was obtained.[20] V_{oc} of 0.67 V has also been obtained using Co redox couples, but the efficiency of the cell was limited by the lower J_{sc} (<5 mA/cm^2) due to diffusion limitation in the electrolyte.[16]

In nanostructured sensitized solar cells, the nanostructured photoanode should have high surface area to increase the amount of sensitizer loading to enhance light harvesting. However, the recombination process is proportional to the electrode surface area. V_{oc} in sensitized solar cells is significantly affected by the recombination process.[12,21−23] A balance between recombination and light harvesting is therefore needed to maximize sensitized solar cell performance. Because QDs have higher extinction coefficient than conventional dyes, the surface area in QDSCs may not need as much increase as in DSCs. In this sense, QDSCs can take advantage of the development of new electrode structures [24−27] to control the recombination process. For this purpose, ZnO NR array is an excellent system as electron transporter material in sensitized solar cells presenting high conductivity, moderate increase in the effective area, and easy and cheap preparation.[28−31] Despite the great potentiality of ZnO for the development of QDSCs,[32] the number of works with this material is significantly lower than the number of papers using TiO_2. The QDSCs using ZnO NWs that present higher V_{oc} have been prepared using presynthesized colloidal QDs linked to ZnO surface by bifunctional molecules.[33,34] They have the inconvenience of low QD loading and consequently low J_{sc} with iodine redox couples, known to be not stable with many QDs.[11] J_{sc} was significantly increased with growing the QDs directly on the ZnO NW surface.[35]

In this work, we report V_{oc} values of 0.77 V by using ZnO nanowire (NW) arrays, sensitized with CdS/CdSe semiconducotrs. CdS and CdSe were directly grown on ZnO NW surface by successive ionic layer adsorption and reaction (SILAR) and chemical bath deposition (CBD), respectively. It is, to our best knowledge, the highest V_{oc} reported for QDSCs.[36] The efficiency is, however, still limited (η = 2.7% under 1 sun conditions) because of relatively low photocurrent. The efficiency was able to be pushed up to 3.0% with a novel photoanode architecture of "pine tree" ZnO NRs on Si NWs hierarchical branched structure (HBS), with higher effective surface than ZnO NW arrays and high light-scattering properties. Most importantly, we show the necessity of exploring new electrode architectures, different from DSCS, to improve the current efficiencies of QDSCs.

Photoanode of the novel 3D hierarchical branched structure (HBS), with ∼1 μm, was prepared as schematically presented in Figure 1a along with its architecture (Figure 1b,c). Figure 2 shows the electron microscopic images for the *n*-Si-NWs on FTO, Si-NW/ZnO-NR pine tree HBS, CdS/CdSe sensitizer-coated structures, and the elemental mapping images. The intrinsic (*i*) Si-NWs were randomly grown on an FTO glass via metal catalyzed vapor−liquid−solid (VLS) method and subsequently doped with PH_3 to make *n*-Si-NWs (Figure 1a) for enhancing the electron conductivity. More information about experimental methods can be found in section S1 of the Supporting Information. The *n*-Si-NWs show identical morphology to *i*-Si-NWs. The *n*-Si-NWs have an average diameter of 30 nm with a diameter distribution between 20 and 50 nm (Figure 2a,b), and their layer thickness was ∼1 μm. The branched ZnO-NRs were directly grown on the Si-NWs forming a pine tree structure via hydrothermal synthetic method without using metal catalyst (Figure 2c,d). Hereafter, we use the term NW for ZnO directly formed on FTO (section S2 of the Supporting Information) and

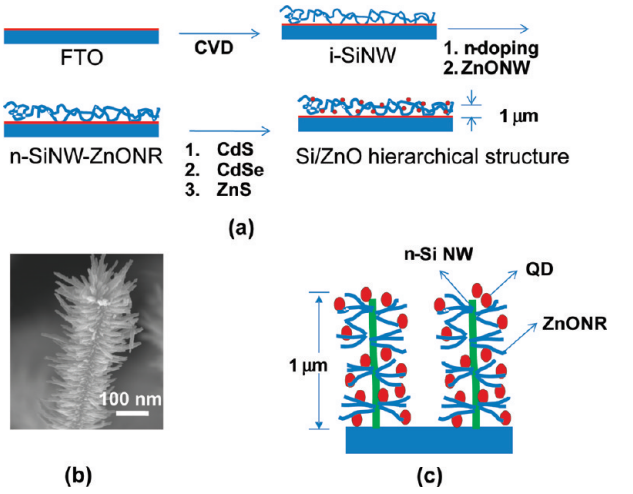

Figure 1. (a) Fabrication scheme of Si/ZnO hierarchical structure, (b) SEM image of *n*-Si-NW/ZnO-NR, and (c) schematic Si/ZnO hierarchical structure for photoanode.

the NR for the ZnO grown on the Si NWs for clarity. ZnO-NRs grew perpendicular to the surface of Si-NWs. HR-TEM image at the top of ZnO-NRs reveals that the ZnO-NRs are single crystalline and were grown along the [001] direction.

CdS QDs were grown directly on ZnO-RD surface by SILAR, and CdSe QDs were deposited by CBD (Figure 2e,f). Finally, ZnS was deposited by SILAR.[37] The total QD-coated layer thickness was of ∼30−35 nm; see section S3 of the Supporting Information. It has been shown that ZnS coating had a good effect in QDSC performance, enhancing significantly the cell photocurrent.[37−39] These methods provide high QD loading and surface coverage.[12,13,16,40] The complete covering of ZnO by CdS/CdSe QDs stabilizes the ZnO, even in the highly basic polysulfide electrolyte (pH ∼13) currently used. Note that the characterization was carried out after 24 h of the QDSC assembly, indicating the stability of the device. The estimated lattice diameter of ca. 0.36 nm confirms that the CdSe was grown along [100] direction. The elemental mapping analysis displays that the sensitizers are homogeneously coated (Figure 2g).

The more detailed SEM image of the 3D ZnO-NR HBS photoanode is presented in section S4 of the Supporting Information. The novel photoanode for QSSCs shows many advantages including: (i) the enhancement in the light-harvesting probability through large surface area for sensitizer loading and photon localization arising from the random multiple scattering of the light within the pine tree network, (ii) the direct charge extraction pathways throughout the device thickness (fast electron transport from sensitizer to collecting terminal), and (iii) the huge 3-D porous network that allows better electrolyte filling, with possible beneficial implications for preparation of solid devices.

The ZnO NW array photoanode increases the effective surface area over the geometric area by a factor of ∼10 but sensibly lower by a factor of 100−1000 than that obtained with nanoporous nanoparticles. This fact will reduce the electron recombination sites markedly compared with a photoanode with nanoporous nanoparticle but decrease the QD loading. This drawback of the low QD loading can be solved using 3D ZnO-NR HBS photoanode with higher effective surface area and high scattering properties. Light scattering can be tuned in ZnO NR arrays by

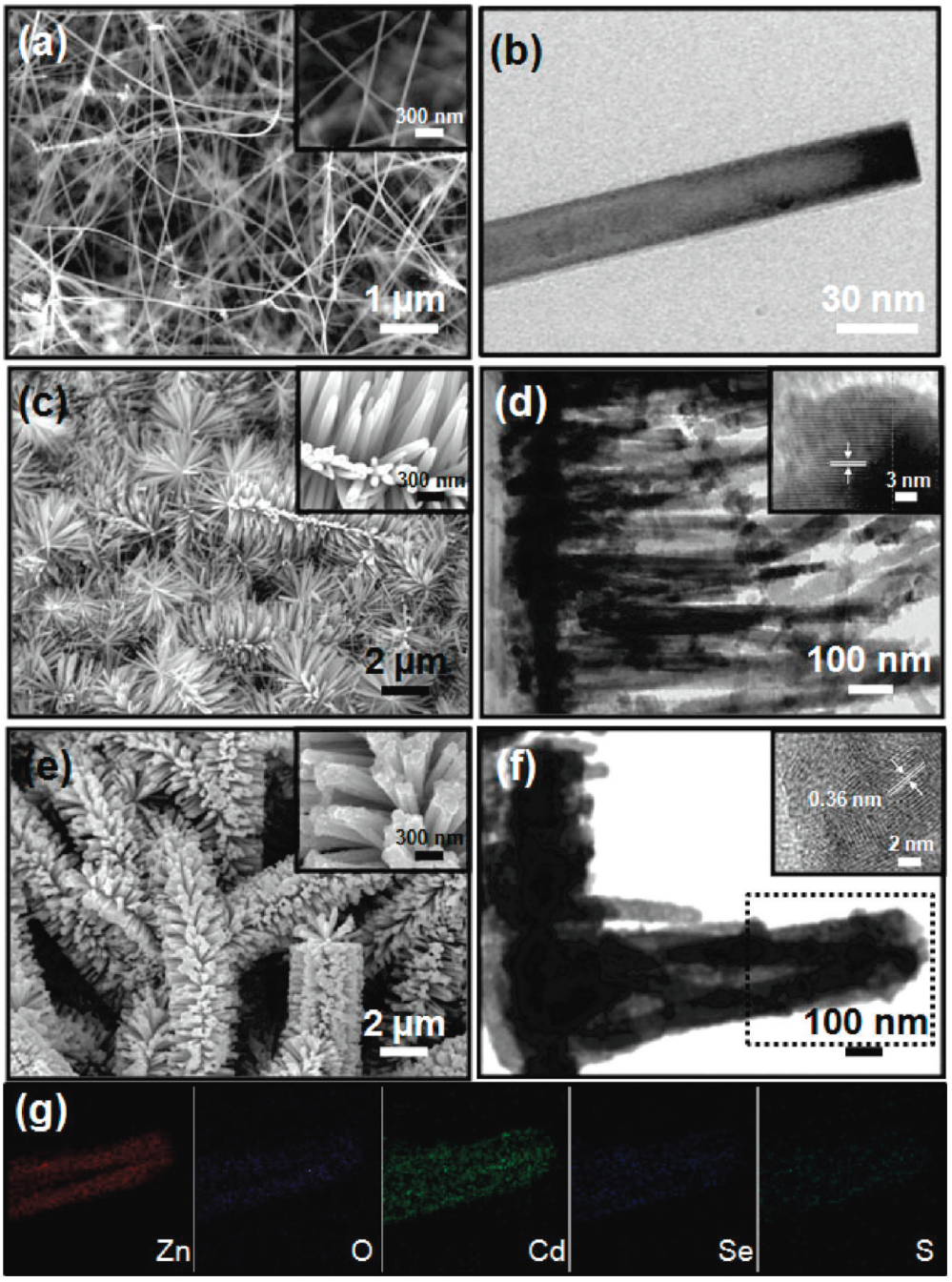

Figure 2. (a) SEM image of *n*-Si-NW on the FTO glass (inset: high magnification SEM image). (b) TEM image of the *n*-Si-NW. (c) SEM image of Si-NW/ZnO-NR pine tree structure (inset: high magnification SEM image). (d) TEM image of the Si-NW/ZnO-NR pine tree structure (inset: high-resolution TEM image at the top of branched ZnO-NR). (e) SEM image after Cds/CdSe coating on the Si-NW/ZnO-NR pine tree structure. (f) TEM image of the CdS/CdSe sensitizer-coated Si-NW/ZnO-NR pine tree structure (inset: high-resolution TEM image of the Cds/CdSe sensitizer). (g) Elemental map of the square box in part f, displaying Zn, O, Cd, Se, and S spatial elemental distribution.

the control of NR length and diameter.[41] In this sense, it could be anticipated that assembling ZnO-RDs on *n*-Si-NW framework offers high light scattering performance. It was also reported that the integration of wide band gap material ZnO ($E_g \approx 3.4$ eV) and narrow band gap Si ($E_g \approx 1.1$ eV) (Si/ZnO) has drawn wider interest in p-n heterojunction devices for efficient photon absorption and conductivity in photovoltaic applications.[26] This novel hierarchical structure of ZnO-NRs with Si-NW pine tree photoanode may therefore have advantages in QDSCs and open a new pathway for exploiting effective alternative photoelectrode architecture with reduced electrode thickness and high light scattering properties.[26]

Photoanodes with ZnO-NW and *n*-Si-NW/ZnO-NR HBS containing CdS/CdSe QDs have been optically analyzed by diffuse reflectance (Figure 3a). Both sensitized electrodes present a decrease in the reflectance for the wavelength shorter than 620 nm due to light absorption of CdS/CdSe sensitizer. Analyzing the reflectance values at longer wavelength, before the absorption

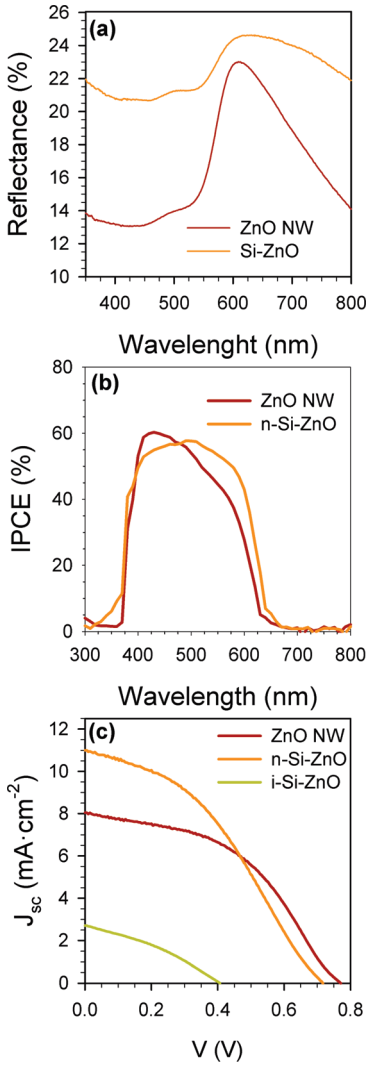

Figure 3. Characteristics of QDSCs using different nanostructured electrodes: ZnO NW, *i*-Si/ZnO, and *n*-Si/ZnO HS with CdS/CdSe QDs. (a) Reflectance, (b) IPCE, and (c) $J-V$ curve.

threshold, the improved scattering properties of the pine tree HBS, in comparison with ZnO-NWs, are manifested in the higher reflection values at these wavelengths.[41] The abortion measurements also indicate that in addition to higher light scattering properties, QD-coated pine tree HBS shows higher QD loading than sensitized ZnO NWs; see section S5 of the Supporting Information. Sensitized electrodes have been used to prepare QDSCs, and the incident photon to current efficiency (IPCE) is plotted in Figure 3b. The IPCE presents a similar threshold to reflectance. It is important to highlight that no significant IPCE is observed at wavelengths longer than 700 nm, indicating a negligible contribution of the Si-NWs to QDSC performance. This fact also suggests that the light absorbed by Si-NWs is negligible and consequently the differences observed in reflectance values at longer wavelength in Figure 4a are in fact due to the scattering properties. The enhanced light scattering is also the responsible of the higher IPCE obtained for pine tree HBS in the wavelength range of 500−650 nm.

Figure 3c plots the current−potential ($J-V$) curves of the prepared QDSCs. The solar cell parameters for each cell are collected in Table 1. A great deal of interesting information can be extracted of this graph: (i) Both ZnO-NW and *n*-Si/ZnO HBS present remarkably high V_{oc} in the case of ZnO-NW, the highest ever reported for liquid QDSCs to the best of our knowledge. (ii) *n*-Si/ZnO HBS QDSC presents higher J_{sc} than ZnO-NW QDSC due to the higher QD loading and the enhanced light-scattering properties of this structure, compensating the relative low J_{sc} obtained with ZnO-NW electrodes. (iii) *i*-Si/ZnO HS QDSC presents significantly lower performance than the other two cells. The photocurrent obtained from the $J-V$ curves is higher than the expected one from IPCE measurements because of two facts: $J-V$ measurements have been carried out without mask and with a reflecting metallic surface after the platinized electrode.

To understand the behavior differences observed between intrinsic and doped Si NWs, we performed electrochemical impedance spectroscopy (IS) measurements of *i*-Si/ZnO and *n*-Si/ZnO HBS, without sensitizer, in a three-electrode cell. The results for applied voltage between −0.3 and −0.55 V versus Ag/AgCl are plotted in Figure 4. There is a clear difference between intrinsic and doped samples. It can be observed especially at higher frequencies. For *i*-Si/ZnO sample, a transmission line (TL) behavior,[22] characterized by a straight line at higher frequencies, followed by a semicircle, is clearly observed (Figure 4c), whereas it is not observed for *n*-Si/ZnO (Figure 4d). No TL behavior has been observed in the highly doped ZnO NWs[30] because of their high conductivity. In this sense, the TL behavior can be attributed to the electron transport in the *i*-Si NW. In contrast, for *n*-Si/ZnO sample, no TL is observed, indicating that the transport resistance along *n*-Si NWs is too small to be detected by this technique. In this sense, doping enhances the transport properties of Si NWs, producing a beneficial effect in *n*-Si/ZnO HBS QDSC performance (Figure 3c).

Impedance measurements have been fitted using the equivalent circuits previously developed for the case with no TL[22,23] (Figure 4e) and with TL[12,22] (Figure 4f). R_s is the series resistance due to contacts, C_μ is chemical capacitance due to the rise of Fermi level, and R_{rec} is the recombination resistance originated by the charge transfers of electrons in the working electrode and acceptor states in the electrolyte, sensitizer layer, or both.[22] TL represents the transmission line, and C_{BL} is the capacitance at the interface between the electrolyte and the uncovered buffer layer of the active electrode.[22] The TL fitting allows us to determine C_μ, R_{rec}, and the transport resistance, R_{tr}, The transport resistance for *i*-Si NWs is plotted in section S6 of the Supporting Information.

To understand the origin of the high open circuit voltage obtained for both ZnO NW and *n*-Si/ZnO HBS, IS of complete solar cell device was carried out. An example of the obtained Nyquist plots and the equivalent circuit employed for their fitting is displayed in section S7 of the Supporting Information. Figure 5 plots C_μ and R_{rec} for complete ZnO NW and *n*-Si/ZnO HBS QDSCs as a function of the voltage drop in the sensitized electrode V_F for the same cells analyzed in the Figure 5. IS enables extracting the voltage drop in the sensitized electrode, V_F, at each applied potential, V_{app}, by subtracting the effect of the series resistance and counter electrode charge transfer resistance on both R_{rec} and C_μ as follows: $V_F = V_{app} - V_s - V_{CE}$, where V_s and V_{CE} are the potential drops at the series resistance and at the counter electrode, respectively.[12,22] For the sake of clarity, $J-V$ performance of QDSC (V_{oc} = 0.55 V, J_{sc} = 13.8 mA·cm^{-2}, FF = 0.50, and η = 3.8%) prepared using a nanoporous electrode from TiO_2 nanoparticles is also added in Figure 5.[12] The TiO_2 nanostructured QDSC also uses CdS/CdSe as sensitizer, but in this case, both were prepared by SILAR method.

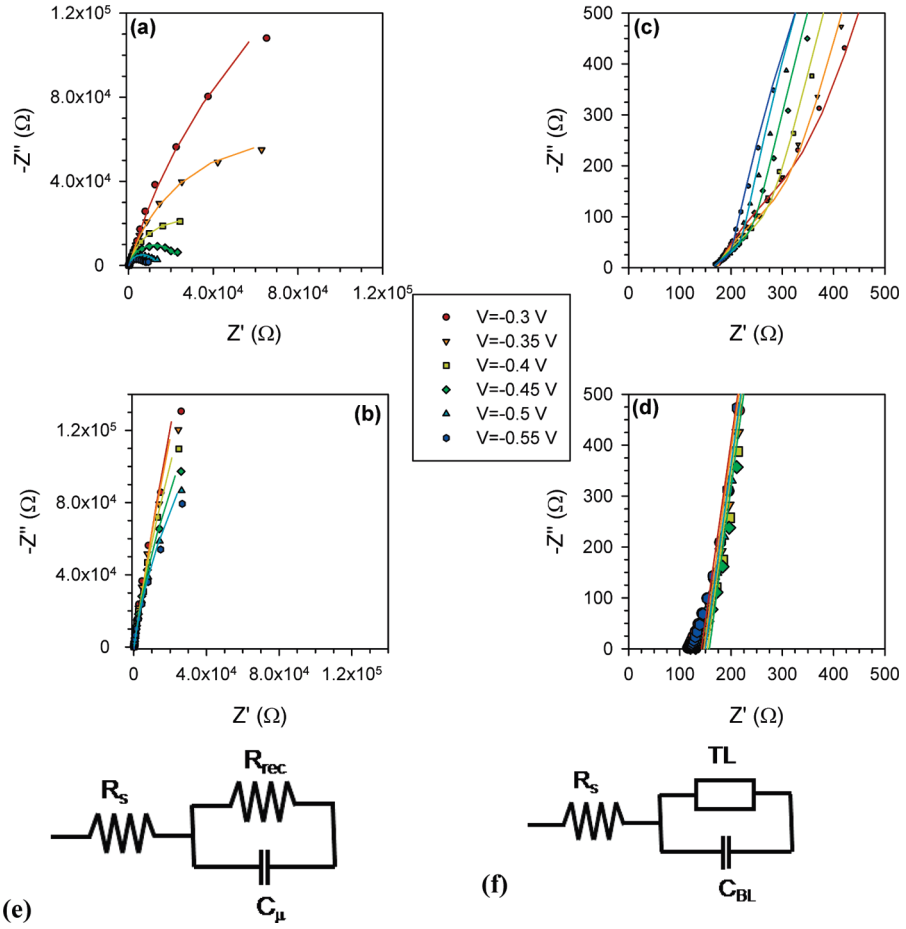

Figure 4. Nyquist plot of obtained from electrochemical impedance measurements for (a) *i*-Si/ZnO HBS and (b) *n*-Si/ZnO HBS. (c,d) Zooms at high-frequency range of parts a and b, respectively. Solid lines correspond to the fit using the equivalent circuits (e) for *i*-Si/ZnO HBS and (f) for *n*-Si/ZnO HBS.[22] Note that in these equivalent circuits the counter electrode does not appear because the impedance measurement was a three-electrode measurement.

Table 1. Photovoltaic Parameters of Semiconductor-Sensitized Solar Cells Using ZnO-NR Arrays and Si with ZnO-NR Pine Tree Hierarchical Branched Photoanode with 1 μm Thickness[a]

samples	Voc (V)	Jsc (mA cm^{-2})	FF [%]	efficiency [%]
ZnO-NR	0.77	8.05	44	2.71
n-Si/ZnO	0.71	11.00	38	3.00
i-Si/ZnO	0.41	2.71	33	0.37

[a] *i*-Si: intrinsic silicon; *n*-Si: n-doped Si.

ZnO NW and *n*-Si/ZnO HS QDSCs present a moderate increase in C_μ with V_F until V_F values of 0.35 and 0.5 V, respectively, as shown in Figure 5a. Then, the capacitance slightly decreased at higher V_F. The moderate increase in C_μ with V_F is the classical signature of doped samples, where the applied voltage can only slightly modify the position of the Fermi level.[22] This is consistent with the n doping of Si and with the high doping reported for ZnO NWs.[30,31] The constant capacitance can be related with a Fermi level pinning,[23] whereas the decrease at higher V_F could be related as a consequence of the appearance of a negative capacitance because it has been discussed elsewhere.[42] *i*-Si/ZnO HS sample also presents a maximum for C_μ but at a lower V_F, showing a significantly higher slope, even higher than the observed for TiO_2 sample. This fact, taking into account the high doping of ZnO, indicates that the Fermi level of intrinsic Si is varying as we charge Si NWs with the applied potential in the same way as the TiO_2 Fermi level is modified in DSCs and QDSCs.[22] Therefore, Si NWs take part in the electron transport process, and the electrons flow through a highly conductive Si NW after photogenerated charge separation at Si/ZnO/CdS/CdSe interfaces. Intrinsic silicon shows poor conductivity, as has been discussed, which restricts the charge transport from ZnO to FTO substrate, reducing the cell performance. Therefore, improved conducting property of *n*-Si pine tree channels allows the rapid electron flow from ZnO to FTO. Finally, note that the largest capacitance value obtained for the TiO_2 sample is due to a higher volume of electron transport material, in comparison with the cells analyzed in this work.

Figure 5b plots the recombination resistance of the cells analyzed, also in comparison with the reference TiO_2 QDSCs. The numerical values of the graph indicate the open circuit voltage measured for each cell under 1 sun illumination (Table 1). Note the intimate relationship between recombination (recombination rate is inversely proportional to R_{rec}) and open circuit potential. A significant increase in R_{rec} for ZnO NW array and *n*-Si/ZnO HBS is observed in comparison with TiO_2 and *i*-Si/ZnO HBS samples, in excellent correlation with the V_{oc} values. This correlation has

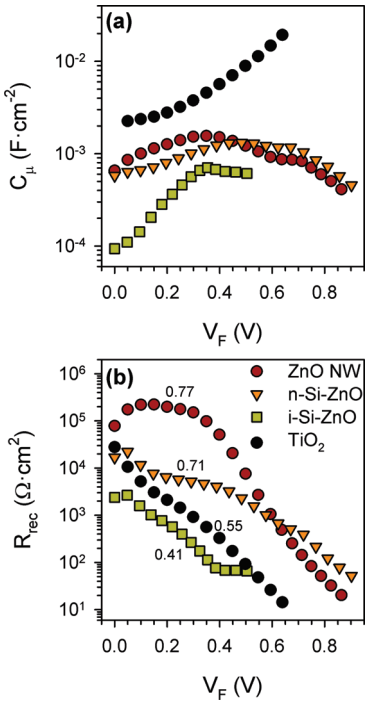

Figure 5. Characteristics for QDSCs using different nanostructured electrodes: ZnO NW, *i*-Si/ZnO, and *n*-Si/ZnO with CdS/CdSe QDs along with a nanostructured TiO_2 as a reference. (a) Chemical capacitance, C_μ, and (b) recombination resistance, R_{rec}, numerical values indicate the open circuit voltage measured for each cell under 1 sun illumination (Table 1). The color code for Figure 5a is the same as that for Figure 5b.

been independently verified by lifetime measurement using V_{oc} decay characterization (section S8, Supporting Information). The larger effective surface area of *n*-Si/ZnO HBS, in comparison with ZnO NW array, produces an increase in recombination, originating the slight decrease in V_{oc} observed for these electrodes. Comparing *i*-Si/ZnO and *n*-Si/ZnO HBS electrodes (without sensitizer) in Figure 4, higher recombination resistance, R_{rec}, is obtained for *n*-Si/ZnO, in good agreement with the results reported for polysulfide electrolyte (Figure 5b). Note that the R_{rec} observed in Figure 4 (diameter of the semicircle) is higher than the reported value in Figure 5b because the electrolyte used for the characterization plotted in Figure 4 does not contain a redox couple. This fact indicates that n doping of Si NWs not only improves the transport properties of the electrode but also reduces the recombination process.

In summary, taking advantage of the high extinction coefficients of semiconductor QDs, recombination process can be reduced decreasing the sensitized electrode surface area, enabling V_{oc} values as high as 0.77 V with a moderate reduction of photocurrents. The photocurrent reduction can be compensated using electrodes with higher effective surface area and high light scattering as the pine tree structures formed with *n*-Si NWs assembled hierarchically by ZnO NR branches, reporting a promising 3% efficiency with 1 μm thickness. Pine tree structures have the additional advantage of the fast electron transport through *n*-Si NWs. More importantly, we show here that it is possible to obtain higher V_{oc} QDSCs with an appropriate treatment of the recombination process, highlighting the fact that QDSCs have to be rethought, separately of DSCs, to optimize their performance. In addition, the technique for fabricating Si/ZnO may be transformed to design potential photoanodes for solar cells based on solid-state electrolyte, water-splitting, and photocatalyst applications.

■ ASSOCIATED CONTENT

Supporting Information. Materials and methods, surface morphology of directly grown ZnO on FTO substrate, QD coated layer, surface morphology of ZnO NR branched structure, light absorption measurements, Nyquist plot of ZnO NW and *n*-Si/ZnO pine tree HBS QDSCs, transport resistance in *i*-Si NWs, and lifetime of ZnO NW and Si/ZnO pine tree HS QDSCs. This material is available free of charge via the Internet at http://pubs.acs.org.

■ AUTHOR INFORMATION

Corresponding Author

*kangys@hanyang.ac.kr (Y.S.K.), upaik@hanyang.ac.kr (U.P.), sero@fca.uji.es (I.M.-S.).

Author Contributions

⊥These authors contributed equally to this work.

■ ACKNOWLEDGMENT

This research was supported by World Class University (WCU) program (R31-2008-000-10092), Engineering Research Center Program (2011-0001055) through Korea Science and Engineering Foundation funded by the Ministry of Education, Science and Technology of Korea, National Research Foundation of Korea through a grant (K2070400000307A050000310, Global Research Laboratory Program) provided by the Korean Ministry of Education, Science and Technology, the Ministerio de Educación y Ciencia of Spain under the projects HOPE CSD2007-00007 (Consolider-Ingenio 2010), JES-NANOSOLAR PLE2009-0042, and MAT 2010-19827 and by Generalitat Valenciana project PROMETEO/2009/058.

■ REFERENCES

(1) Kamat, P. V. Quantum Dot Solar Cells. Semiconductor Nanocrystals as Light Harvesters. *J. Phys. Chem. C* **2008**, *112*, 18737–18753.

(2) Kamat, P. V.; Tvrdy, K.; Baker, D. R.; Radich, J. G. Beyond Photovoltaics: Semiconductor Nanoarchitectures for Liquid-Junction Solar Cells. *Chem. Rev.* **2010**, *110*, 6664–6688.

(3) Mora-Seró, I.; Bisquert, J. Breakthroughs in the Development of Semiconductor-Sensitized Solar Cells. *J. Phys. Chem. Lett.* **2010**, *1*, 3046–3052.

(4) Rühle, S.; Shalom, M.; Zaban, A. Quantum-Dot-Sensitized Solar Cells. *Chem. Phys. Chem.* **2010**, *11*, 2290–2304.

(5) O' Regan, B.; Grätzel, M. A Low-Cost High-Efficiency Solar Cell Based on Dye-Sensitized Colloidal TiO_2 Films. *Nature* **1991**, *353*, 737.

(6) Gao, F.; Wang, Y.; Shi, D.; Zhang, J.; Wang, M.; Jing, X.; Humphry-Baker, R.; Wang, P.; Zakeeruddin, S. M.; Grätzel, M. Enhance the Optical Absorptivity of Nanocrystalline TiO_2 Film with High Molar Extinction Coefficient Ruthenium Sensitizers for High Performance Dye-Sensitized Solar Cells. *J. Am. Chem. Soc.* **2008**, *130*, 10720–10728.

(7) Yu, Q.; Wang, Y.; Yi, Z.; Zu, N.; Zhang, J.; Zhang, M.; Wang, P. High-Efficiency Dye-Sensitized Solar Cells: The Influence of Lithium Ions on Exciton Dissociation, Charge Recombination, and Surface States. *ACS Nano* **2010**, *4*, 6032–6038.

(8) Yu, W.; Qu, L. H.; Guo, W. Z.; Peng, X. G. Experimental Determination of the Extinction Coefficient of CdTe, CdSe, and CdS Nanocrystals. *Chem. Mater.* **2003**, *15*, 2854–2860.

(9) Alivisatos, A. P. Semiconductor Clusters, Nanocrystals, and Quantum Dots. *Science* **1996**, *271*, 933–937.
(10) Sambur, J. B.; Novet, T.; Parkinson, B. A. Multiple Exciton Collection in a Sensitized Photovoltaic System. *Science* **2010**, *330*, 63–66.
(11) Hodes, G. Comparison of Dye- and Semiconductor-Sensitized Porous Nanocrystalline Liquid Junction Solar Cells. *J. Phys. Chem. C* **2008**, *112*, 17778–17787.
(12) Gónzalez-Pedro, V.; Xu, X.; Mora-Seró, I.; Bisquert, J. Modeling High-Efficiency Quantum Dot Sensitized Solar Cells. *ACS Nano* **2010**, *4*, 5783–5790.
(13) Zhang, Q.; Guo, X.; Huang, X.; Huang, S.; Li, D.; Luo, Y.; Shen, Q.; Toyoda, T.; Meng, Q. Highly Efficient CdS/CdSe-Sensitized Solar Cells Controlled by the Structural Properties of Compact Porous TiO_2 Photoelectrodes. *Phys. Chem. Chem. Phys.* **2011**, *13*, 4659–4667.
(14) Chang, J. A.; Rhee, J. H.; Im, S. H.; Lee, Y. H.; Kim, H.-J.; Seok, S. I.; Nazeeruddin, M. K.; Grätzel, M. High-Performance Nanostructured Inorganic−Organic Heterojunction Solar Cells. *Nano Lett.* **2010**, *10*, 2609–2612.
(15) Hossain, M. A.; Jennings, J. R.; Koh, Z. Y.; Wang, Q. Carrier Generation and Collection in CdS/CdSe-Sensitized SnO_2 Solar Cells Exhibiting Unprecedented Photocurrent Densities. *ACS Nano* **2011**, *5*, 3172–3181.
(16) Lee, H. J.; Wang, M.; Chen, P.; Gamelin, D. R.; Zakeeruddin, S. M.; Grätzel, M.; Nazeeruddin, M. K. Efficient CdSe Quantum Dot-Sensitized Solar Cells Prepared by an Improved Successive Ionic Layer Adsorption and Reaction Process. *Nano Lett.* **2009**, *9*, 4221–4227.
(17) Lee, H. J.; Yum, J.-H.; Leventis, H. C.; Zakeeruddin, S. M.; Haque, S. A.; Chen, P.; Seok, S. I.; Grätzel, M.; Nazeeruddin, M. K. CdSe Quantum Dot-Sensitized Solar Cells Exceeding Efficiency 1% at Full-Sun Intensity. *J. Phys. Chem. C* **2008**, *112*, 11600–11608.
(18) Tachan, Z.; Shalom, M.; Hod, I.; Rühle, S.; Tirosh, S.; Zaban, A. PbS as a Highly Catalytic Counter Electrode for Polysulfide-Based Quantum Dot Solar Cells. *J. Phys. Chem. C* **2011**, *115*, 6162–6166.
(19) Sudhagar, P.; Jung, J. H.; Park, S.; Lee, Y.-L.; Sathyamoorthy, R.; Kang, Y. S.; Ahn, H. The Performance of Coupled (CdS:CdSe) Quantum Dot-Sensitized TiO_2 Nanofibrous Solar Cells. *Electrochem. Commun.* **2009**, *11*, 2220–2224.
(20) Diguna, L. J.; Shen, Q.; Kobayashi, J.; Toyoda, T. High Efficiency of CdSe Quantum-Dot-Sensitized TiO_2 Inverse Opal Solar Cells. *Appl. Phys. Lett.* **2007**, *91*, 023116.
(21) Barea, E. M.; Shalom, M.; Giménez, S.; Hod, I.; Mora-Seró, I.; Zaban, A.; Bisquert, J. Design of Injection and Recombination in Quantum Dot Sensitized Solar Cells. *J. Am. Chem. Soc.* **2010**, *132*, 6834–6839.
(22) Fabregat-Santiago, F.; Garcia-Belmonte, G.; Mora-Seró, I.; Bisquert, J. Characterization of Nanostructured Hybrid and Organic Solar Cells by Impedance spectroscopy. *Phys. Chem. Chem. Phys.* **2011**, *13*, 9083–9118.
(23) Mora-Seró, I.; Giménez, S.; Fabregat-Santiago, F.; Gómez, R.; Shen, Q.; Toyoda, T.; Bisquert, J. Recombination in Quantum Dot Sensitized Solar Cells. *Acc. Chem. Res.* **2009**, *42*, 1848–1857.
(24) Choi, K.-S. Shape Effect and Shape Control of Polycrystalline Semiconductor Electrodes for Use in Photoelectrochemical Cells. *J. Phys. Chem. Lett.* **2010**, *1*, 2244–2250.
(25) Jin, S.; Bierman, M. J.; Morin, S. A. A New Twist on Nanowire Formation: Screw-Dislocation-Driven Growth of Nanowires and Nanotubes. *J. Phys. Chem. Lett.* **2010**, *1*, 1472–1480.
(26) Devika, M.; Reddy, N. K.; Pevzner, A.; Patolsky, F. Hetero-epitaxial Si/ZnO Hierarchical Nanostructures for Future Optoelectronic Devices. *Chem. Phys. Chem.* **2010**, *11*, 809–814.
(27) Patolsky, F.; Zheng, G.; Lieber, C. M. Fabrication of Silicon Nanowire Devices for Ultrasensitive, Label-Free, Real-Time Detection of Biological and Chemical Species. *Nat. Protoc.* **2006**, *1*, 1711–1724.
(28) Krunks, M.; Karber, E.; Katerski, A.; Otto, K.; Oja Acik, I.; Dedova, T.; Mere, A. Extremely Thin Absorber Layer Solar Cells on Zinc Oxide Nanorods by Chemical Spray. *Sol. Energy Mater. Sol. Cells* **2010**, *94*, 1191–1195.
(29) Lévy-Clément, C.; Tena-Zaera, R.; Ryan, M. A.; Katty, A.; Hodes, G. CdSe- Sensitized p-CuSCN/Nanowire n-ZnO Heterojunctions. *Adv. Mater.* **2005**, *17*, 1512–1515.
(30) Mora-Seró, I.; Fabregat-Santiago, F.; Denier, B.; Bisquert, J.; Tena-Zaera, R.; Elias, J.; Lévy-Clément, C. Determination of Carrier Density of ZnO Nanowires by Electrochemical Techniques. *Appl. Phys. Lett.* **2006**, *89*, 203117.
(31) Tena-Zaera, R.; Elias, J.; Lévy-Clément, C.; Bekeny, C.; Voss, T.; Mora-Seró, I.; Bisquert, J. Influence of the Potassium Chloride Concentration on the Physical Properties of Electrodeposited ZnO Nanowire Arrays. *J. Phys. Chem. C* **2008**, *112*, 16318–16323.
(32) Barceló, I.; Lana-Villarreal, T.; Gómez, R. Efficient Sensitization of ZnO Nanoporous Films with CdSe QDs Grown by Successive Ionic Layer Adsorption and Reaction (SILAR). *J. Photoch. Photobio. A* **2011**, *220*, 47–53.
(33) Leschkies, S. K.; Divakar, R.; Basu, J.; Enache-Pommer, E.; Boercker, J. E.; Carter, C. B.; Kortshagen, U. R.; Norris, D. J.; Aydil, E. S. Photosensitization of ZnO Nanowires with CdSe Quantum Dots for Photovoltaic Devices. *Nano Lett.* **2007**, *7*, 1793–1798.
(34) Rogach, A.; Luan, C.; Vaneski, A.; Susha, A.; Xu, X.; Wang, H.-E.; Chen, X.; Zhang, W.; Xu, J.; Lee, C.-S.; et al. Facile Solution Growth of Vertically Aligned ZnO Nanorods Sensitized with Aqueous CdS and CdSe Quantum Dots for Photovoltaic Applications. *Nanoscale Res. Lett.* **2011**, *6*, 340.
(35) Seol, M.; Kim, H.; Tak, Y.; Yong, K. Novel Nanowire Array Based Highly Efficient Quantum Dot Sensitized Solar Cell. *Chem. Commun* **2010**, *46*, 5521–5523.
(36) We note that the reported Voc of 1.55 V (*J. Mater. Chem.* **2009**, *19*, 5945−5951) is based on an incorrect data analysis because they use three electrode measurements.
(37) Shen, Q.; Kobayashi, J.; Diguna, L. J.; Toyoda, T. Effect of ZnS Coating on the Photovoltaic Properties of CdSe Quantum Dot-Sensitized Solar Cells. *J. Appl. Phys.* **2008**, *103*, 084304.
(38) Giménez, S.; Mora-Seró, I.; Macor, L.; Guijarro, N.; Lana-Villarreal, T.; Gómez, R.; Diguna, L. J.; Shen, Q.; Toyoda, T.; Bisquert, J. Improving the Performance of Colloidal Quantum Dot Sensitized Solar Cells. *Nanotechnology* **2009**, *20*, 295204.
(39) Guijarro, N.; Campiña, J. M.; Shen, Q.; Toyoda, T.; Lana-Villarreal, T.; Gómez, R. Uncovering the Role of the ZnS Treatment in the Performance of Quantum Dot Sensitized Solar Cells. *Phys. Chem. Chem. Phys.* **2011**, *13*, 12024–12032.
(40) Guijarro, N.; Lana-Villarreal, T.; Shen, Q.; Toyoda, T.; Gómez, R. Sensitization of Titanium Dioxide Photoanodes with Cadmium Selenide Quantum Dots Prepared by SILAR: Photoelectrochemical and Carrier Dynamics Studies. *J. Phys. Chem. C* **2010**, *114*, 21928–21937.
(41) Tena-Zaera, R.; Elias, J.; Lévy-Clément, C. ZnO Nanowire Arrays: Optical Scattering and Sensitization to Solar Light. *Appl. Phys. Lett.* **2008**, *93*, 233119.
(42) Mora-Seró, I.; Bisquert, J.; Fabregat-Santiago, F.; Garcia-Belmonte, G.; Zoppi, G.; Durose, K.; Proskuryakov, Y.; Oja, I.; Belaidi, A.; Dittrich, T.; et al. Implications of the Negative Capacitance Observed at Forward Bias in Nanocomposite and Polycrystalline Solar Cells. *Nano Lett.* **2006**, *6*, 640–650.